

DFN Variability Analysis through Voxelization

Junkin, W.R.

MIRARCO Mining Innovation, Sudbury, Ontario, Canada

Laurentian University, Sudbury, Ontario, Canada

Ben-Awuah, E.

Laurentian University, Sudbury, Ontario, Canada

Fava, L.

MIRARCO Mining Innovation, Sudbury, Ontario, Canada

Copyright 2019 ARMA, American Rock Mechanics Association

This paper was prepared for presentation at the 53rd US Rock Mechanics/Geomechanics Symposium held in New York, NY, USA, 23–26 June 2019. This paper was selected for presentation at the symposium by an ARMA Technical Program Committee based on a technical and critical review of the paper by a minimum of two technical reviewers. The material, as presented, does not necessarily reflect any position of ARMA, its officers, or members. Electronic reproduction, distribution, or storage of any part of this paper for commercial purposes without the written consent of ARMA is prohibited. Permission to reproduce in print is restricted to an abstract of not more than 200 words; illustrations may not be copied. The abstract must contain conspicuous acknowledgement of where and by whom the paper was presented.

ABSTRACT: A fracture network model provides a wealth of information concerning the characteristics of a rock mass, including fracture intensity, block size, and connectivity. This paper identifies methods to utilize information derived from DFN models. The fracture intensity of a DFN can be analysed for individual or grouped subvolumes of the model. A DFN is discretized into volumetric elements (voxels). Stochastic DFN models measuring $25 \times 25 \times 25 \text{ m}^3$ are modeled with identical attributes. Fractures are modeled as non-planar and non-persistent, and orientations varied to generate a variety of block shapes and sizes. The voxels used for metrics analysis range in size from 1 m^3 to $1\,953 \text{ m}^3$, representing from 2^3 to 25^3 voxels. Fracture intensity is measured as a P_{32} value for all elements. The coefficient of variation (CV%) of fracture intensity is calculated for each voxelization to generate a curve characteristic of a particular DFN model. An estimate of the in situ block size distribution (IBSD) is made by considering the number of unfractured voxels (null blocks). The fracture intensity, CV% of fracture intensity and IBSD values derived from these DFNs can be used as input to a variety of secondary models.

1. INTRODUCTION

The MoFrac discrete fracture network (DFN) modeling software (MIRARCO, 2019) implements a rules-based methodology to generate plausible fracture networks guided by information derived from mapped data. (Junkin, *et al.*, 2017; 2018). DFN models can range from entirely stochastic to highly constrained to known data. Information concerning the characteristics of a rock mass can be derived from a DFN model; this includes, *inter alia*, fracture intensity, block size, and flow connectivity. This paper demonstrates a method, through voxelization, to derive information regarding fracture intensity variability and *in situ* block size distribution (IBSD) of DFN models useful for incorporating into secondary studies such as hydrogeological flow, fragmentation, and slope stability analysis.

MoFrac can generate DFN models entirely stochastically, or constrained by known fracture locations and orientations. Stochastic fractures in the models do not rely on any geological mapping, and are defined through orientation, size, and intensity distributions for each fracture set over specified regions. This study considers entirely stochastic DFN models defined over a single region. While the input values for the primary properties

of the DFN model remain constant, variability in the DFN model is expected as a result of the Poisson point process used for seeding fractures.

A metrics analysis package built-in to MoFrac allows for consideration of a DFNs fit to any mapped data, and also allows for statistical analysis of modeled fracture attributes. The metrics also allow for the sampling of a DFN model over given planes or volumes, allowing for the analysis of separate and discrete regions of a DFN model.

By discretizing a DFN model into component cubes, a measure of variation in fracture intensity and an estimation of the IBSD are feasible. The limit to the minimum size and thus maximum number of samples (cubes) is the available computational power. Sampling a DFN discretized 100 times on each axis results in 1 000 000 calculations of fracture intensity in a given volume. This involves cutting fracture surfaces at the boundaries of all sampled volumes.

The calculation of the IBSD from a DFN is also computationally demanding. The Ray Cast Volume algorithm is a simple method used to estimate IBSD from

a DFN but is limited by its ability to detect concave blocks as it involves casting linear rays from random points within the DFN model (Medinac, 2018). Latham *et al.* (2006) discuss several methods of estimating block size distribution within a rock mass and their associated limitations. The ability to generate an entire IBSD assessment from a fracture network model is advantageous as pre-existing data can be utilized. Assessing the entire IBSD from a fracture network can lead to accurate results. Other methods of estimation can be biased by mapping protocols and limited data. Currently, the unavailability of efficient algorithms limit the ability to conduct IBSD assessment using a DFN model.

2. DFN VOXELIZATION

A voxel is a volumetric element of a regular grid in three dimensional space. Voxels generally constitute an array of discrete elements that represent a three dimensional object (Cohen-Or and Kaufman, 1995). For the purpose of this study, the three dimensional object is a DFN model that measures $25 \times 25 \times 25 \text{ m}^3$ ($15\,625 \text{ m}^3$). The size of a voxel is inversely proportional to the number of subdivisions on each axis of the Cartesian coordinate system. The DFN models will be divided equally along each axis, resulting in cubic voxels. Table 1 gives the size of a single voxel in relation to the number of subdivisions of each axis for the $15\,625 \text{ m}^3$ DFN model used for this study. The process of voxelization allows for a DFN model to be discretized in the form of a block model with the number of blocks equal to the number of voxels.

Table 1. Voxel size in relation to the number of subdivisions of a $25 \times 25 \times 25 \text{ m}^3$ volume.

Subdivisions per Axis	# of Voxels	Size of Voxel (m^3)
1	1	15 625
5	125	125
10	1 000	15.62
15	3 375	4.63
20	8 000	1.95
25	15 625	1

The goal of this study is to develop a methodology for measuring the heterogeneity of DFNs in a way that facilitates comparisons between models. Voxelization allows for spatial analysis at multiple scales. The property of interest for each voxel is the P_{32} fracture intensity. P_{32} intensity is the sum of the surface areas of fractures within a given volume divided by that volume, calculated as shown in Equation (1) (Rogers, *et al.*, 2009).

$$P_{32} = \frac{\sum_1^n A}{V} \quad (1)$$

The benefit of using P_{32} intensities to characterize a DFN is that this measure is scale-independent, and there is no bias related to the direction of measurement, as occurs with P_{21} values (Dershowitz and Herda, 1992; Alghalandis and Elmo, 2018).

The P_{32} intensity of DFN models will be considered for ten realizations of the stochastic DFN model defined in Section 3. To analyze the DFN models, 1 through 25 subdivisions are used. Figure 1 shows an example of a simple cube subdivided into 1000 component voxels (10^3).

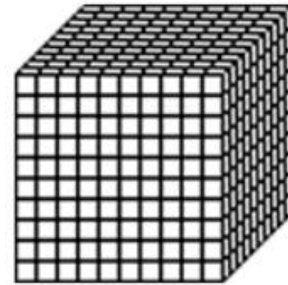


Figure 1. Example of a $10 \times 10 \times 10$ voxelization of a simple cube resulting in 1000 voxels.

3. STOCHASTIC DFN RECIPE

Ten realizations of a completely stochastic DFN model were generated using MoFrac. The primary properties used for modeling include orientation, size, and intensity distributions. The DFN is defined over a single homogenous domain; there is no spatial variation with inputs. Fractures are seeded using a Poisson point process and no truncations or terminations are defined; minimum and maximum fracture size are defined inputs. The primary properties required for basic DFN modeling are defined and described below (Dershowitz, *et al.*, 2017).

The size of the DFN model is $25 \times 25 \times 25 \text{ m}^3$, for a total volume of $15\,625 \text{ m}^3$. Three fracture sets are defined. Fracture sets A and B are dipping subvertically; fracture set A is defined as striking North-South and fracture set B is defined as striking East-West. Fracture set C dips subhorizontally. The input fracture orientation assumes a Gaussian distribution and is defined by a strike and dip for each fracture set with an associated standard deviation (SD) for each value. The orientation inputs for each are given in Table 2.

Table 2. Input orientations and standard deviations for each fracture set in the stochastic DFN model.

Fracture set	Strike	SD of strike	Dip	SD of dip
A	0°	15°	90°	15°
B	90°	15°	90°	15°
C	35°	15°	0°	5°

The fracture size distribution is guided by a power law distribution, and is defined as two points on a cumulative area distribution (CAD) curve. X_1 and X_2 are the numbers of fractures $>$ threshold by volume and A_1 and A_2 are the fracture surface areas for the associated X values. The area samples used to generate fractures are based on a uniform sampling with randomization of the sampled area to allow for variety between realizations. A minimum fracture surface size of 50 m^2 and a maximum fracture surface size of 100 m^2 is defined as an input. The fracture size and intensity inputs are given in Table 3.

Table 3. Size and intensity inputs and P_{32} output for each fracture set in the stochastic DFN model.

Fracture Set	Min Size (m^2)	Max Size (m^2)	X_1	A_1 (m^2)	X_2	A_2 (m^2)	P_{32} (m^{-1})
A	50	100	0.004	50	0.002	100	0.35
B	50	100	0.005	50	0.003	100	0.35
C	50	100	0.006	50	0.004	100	0.46

Secondary properties defined for the DFN models are required inputs for MoFrac, and are summarized in Table 4. Fracture truncations are defined as a probability of termination between each pair of fracture sets; no truncations are defined for this model. Stochastic fractures have their size limited explicitly. The strike to dip ratio controls the aspect ratio of the fracture shape. It defines the limits of the ratio of fracture strike length to fracture dip length. The undulation value allows for surface waviness of the fracture. The degree of waviness is unitless and a relative scale normalized from 0 to 1. The degree of undulation is also determined by the triangle size, as the undulation parameter controls fracture mesh tessellation. All reported fracture surface areas are based on a planar realization of an undulated fracture; the additional area associated with undulation is not included.

Table 4. Secondary properties used for DFN modeling.

Fracture set	A	B	C
Min strike to dip ratio	1	1	1
Max strike to dip ratio	5	5	5
Fracture shape	Elliptical	Elliptical	Elliptical
Undulation	0.25	0.25	0.25
Truncation	0 %	0 %	0 %
Triangle Size	100 m^2		

Ten realizations of the DFN model were generated for further analysis. A single realization is shown in Figure 2; each fracture set is shown individually, as well as the whole DFN model. Slices passing through the center of the model on the XY, XZ and YZ plane are also shown. P_{21} values for each realization on these planes are given in Table 5 along with P_{32} values for each DFN as a whole.

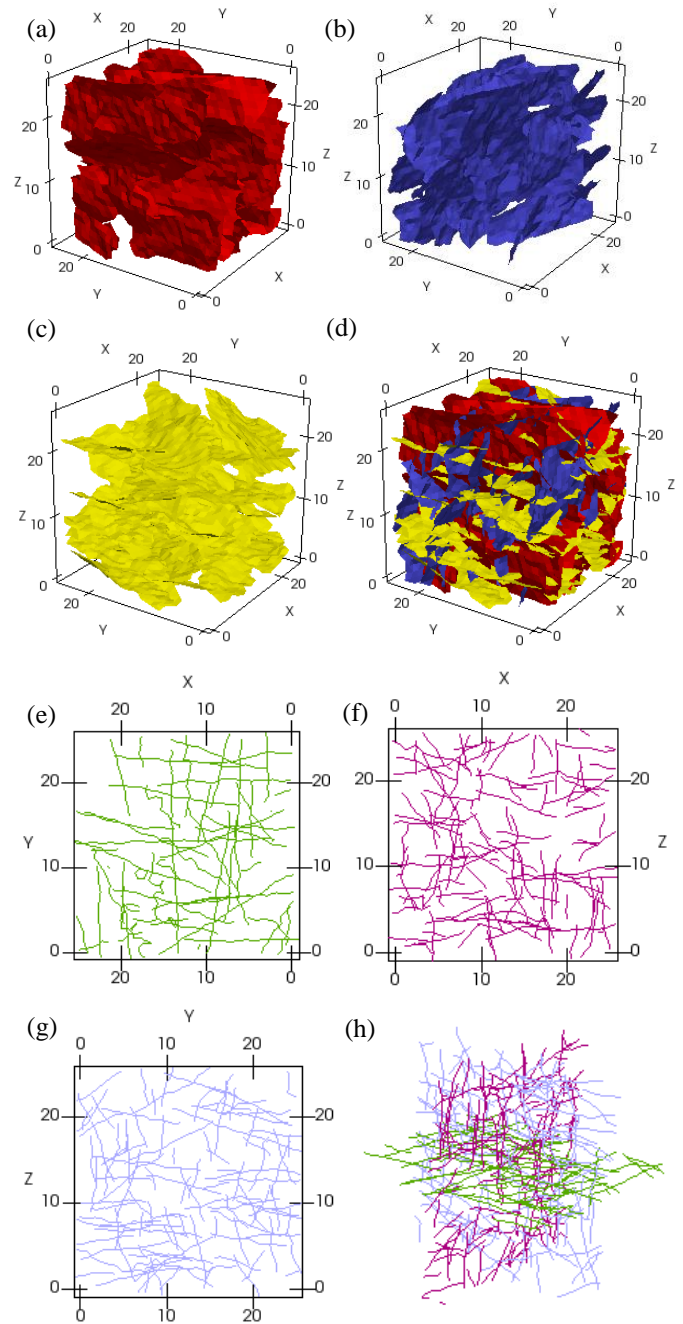


Figure 2. Visual representation of a single DFN realization. (a) Fracture set A, (b) fracture set B, (c) fracture set H, and (d) the entire DFN model with slices in the (e) XY plane, (f) XZ plane, (g) YZ plane, and (h) all three planes.

4. DFN BOUNDARY EFFECT

An analysis of any potential boundary effect should be carried out before a DFN is accepted as representative of a rock mass. The boundary effect is caused by the fact that some fractures that would be seeded just out of bounds and would propagate into the DFN model are not included in the model, reducing fracture intensity at the boundaries. This can be rectified by increasing fracture intensity at boundaries using simulated mapped fracture traces.

Table 5. P_{21} and P_{32} fracture intensities for the DFN models

DFN model	P_{21} XY plane	P_{21} XZ plane	P_{21} YZ plane	P_{32}
1	0.84	1.04	1.12	1.20
2	0.70	1.06	1.05	1.18
3	0.93	1.12	1.11	1.19
4	0.99	1.09	1.05	1.20
5	1.05	1.06	0.95	1.19
6	0.69	1.08	1.06	1.21
7	0.82	1.13	1.06	1.19
8	0.72	1.15	1.05	1.20
9	0.93	1.10	1.13	1.21
10	0.94	1.11	1.10	1.19
Mean	0.86	1.09	1.07	1.20
Standard Deviation	0.1273	0.0333	0.0517	0.0083

The boundary effect for a DFN model is quantified by considering the difference in P_{32} fracture intensities between interior and exterior regions of the DFN model as shown in Figure 3.

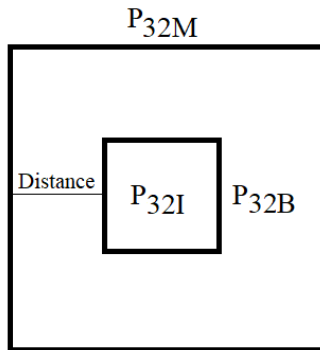


Figure 3. Schematic showing the regions used to quantify the DFN boundary effect.

The process of determining the boundary effect considered preliminary boundary distances of 1 – 8 m. The P_{32} of the model as a whole (P_{32M}), the interior region (P_{32I}), and the boundary region (P_{32B}) are all calculated in order to quantify the extent of the boundary effect. By plotting $P_{32M} - P_{32B}$ the differences in fracture intensity can be compared. The boundary effect extends to the point where the difference between P_{32M} and P_{32B} is a maximum. Past this point there is sufficient fracture intensity in the boundary region to reduce the difference in intensities. Figure 4 shows the curves for the calculated differences in intensity with respect to the linear distance from the DFN boundary to the interior inspection box. A boundary effect of 3.8 m is calculated when data for all ten DFN realizations is considered.

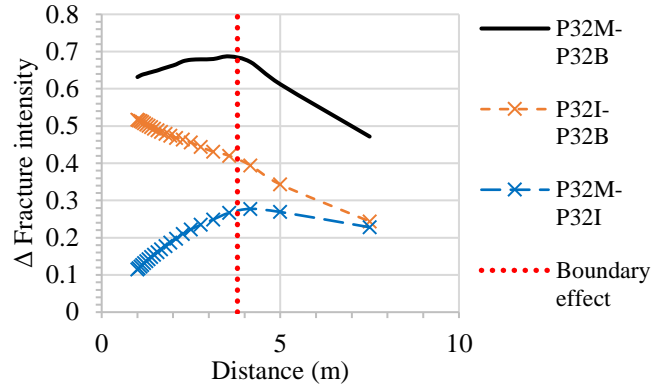


Figure 4. The quantification of the boundary effect for all ten realizations of the DFN model.

Where DFN models are identified as having a change in fracture intensity resulting from a boundary effect, special care should be taken when considering application of the model. Having an underestimation of fracture intensity at boundaries could have significant effect on the conclusions from secondary studies using the DFN models. It is desirable to have mapped traces or fracture seeds on the exterior boundaries of a DFN model to mitigate this risk on modelling outcomes. Where faces are not visible for geological mapping, two simple solutions can be used. A slice through the center of a DFN can be used to estimate the P_{21} fracture intensity where the boundary effect does not exist. This fracture intensity can then be used to stochastically seed fracture traces on the boundaries of a DFN model. Where fracture mapping is possible, the actual fracture traces can be used for seeding on visible faces. The P_{21} of mapped fractures can then be used to stochastically seed opposing faces that are hidden by the rock mass. This allows for increased utilization of information derived from fracture mapping.

5. COEFFICIENT OF VARIATION

The coefficient of variation (CV%) is a measure of the variability of a set of numbers. This variability is independent of the unit of measurement, and CV% is applicable for comparison of data on multiple scales and/or using different measurement systems (e.g., metric or imperial). CV% is calculated by dividing the standard deviation for a population of numbers by the mean; the CV% only applies meaningfully to variables with a real zero (Abdi, 2010); thus, applicable to P_{32} fracture intensities. When $CV\% > 1$, the sample of numbers is considered to have high variability, and when $CV\% < 1$ the sample of numbers is considered to have low variability. The threshold at which variability is considered significant can be adjusted according to the statistics of a DFN model. High variability should be considered relative to the overall variability of the model.

Coefficients of fracture intensity variability are calculated for each voxelization considered in Section 2. The CV% values are calculated based on the entire population of P_{32} values, thus there is no sampling bias. It is expected that, as the sampled volumes decrease, the CV% will increase. The rate at which the CV% increases with a reduction in volume can be plotted as a curve that is characteristic to the DFN model (Min, *et al.*, 2004). This characteristic plot can be used to analyze a specific DFN and to compare one DFN to another. This presents an opportunity to use the CV% curve as a validation for a stochastic DFN based on mapped data.

Figure 5 shows the CV% curve for ten realizations of the same stochastic DFN model as described. The red line shows the average CV% for each data point. The CV% curves for individual realizations are in agreement with one another. Despite this fact, the P_{21} values on identical planes can vary significantly between realizations. This demonstrates that the CV% curve is a global attribute for a DFN model and has potential as a tool for model calibration.

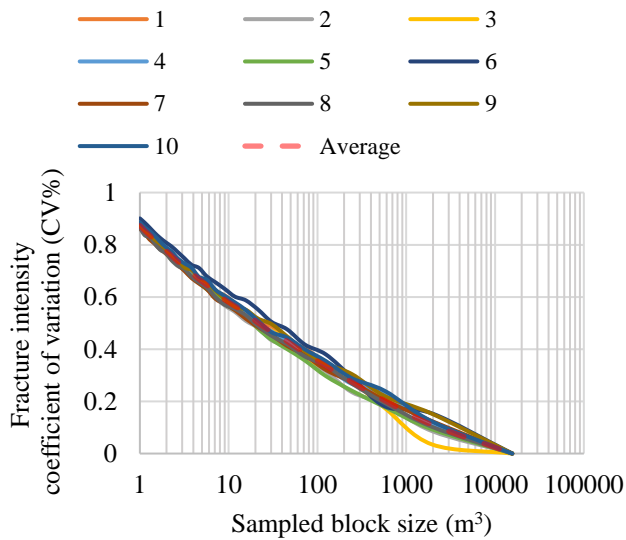


Figure 5. Relation between sampled block size and fracture intensity coefficient of variation for stochastic DFN model on a semi-log plot.

The information derived by analysis of individual voxels within a DFN can also be used to allow for visualization of fracture intensity variation within a DFN. This is demonstrated through the creation of a fracture intensity map for a horizontal section of a DFN model. Figure 6 shows the variation in fracture intensity when considering a voxelization of $10 \times 10 \times 10$ for a single realization. A single square in this fracture intensity heat map represents a voxel that is 15.62 m^3 , with a face area of 6.25 m^2 . The fracture intensity variability is shown visually by means of a heat map. The values for each fracture intensity bin

and associated color are given in Table 5, with the resulting fracture intensity heat map shown in Figure 6. A blue square indicates a null block, meaning that no fractures are present. The spatial arrangement of null blocks across an entire DFN model allows for an estimation of the IBSD. The heat map can be visually checked by overlaying fracture traces from the same DFN slice, as shown in Figure 6.

The variation in P_{32} intensities can be shown with a histogram. Figure 7 shows how the variation in P_{32} is dependent upon the sampled voxel size. Histograms are shown for 25 (1 m^3 voxels), 15 (4.63 m^3 voxels), and 5 (125 m^3 voxels) divisions per axis.

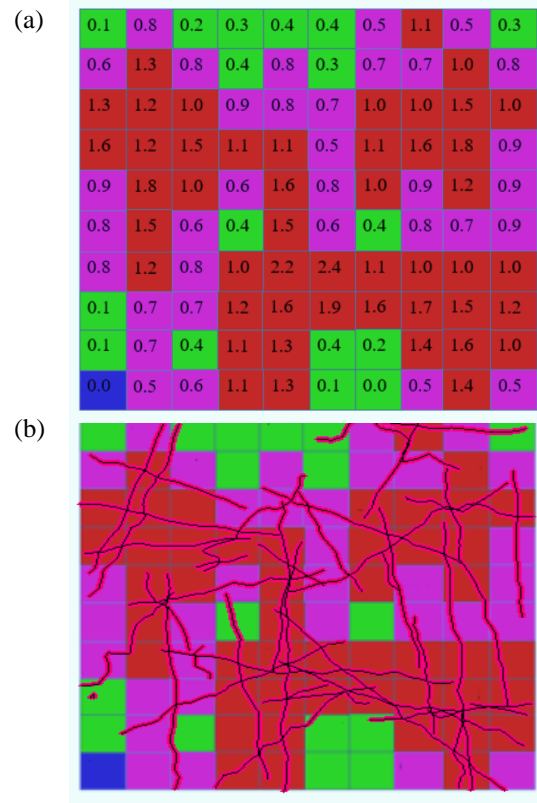


Figure 6. Fracture intensity heat map for a DFN slice from $z = 0$ to $z = 2.5$ with colors as defined in Table 5. Heat map (a) with P_{32} values and (b) with fracture traces from $z = 1.25$. (Table 5 is to be used as a legend)

Table 5. Fracture intensity bins for heat mapping (legend for Figure 6).

Fracture intensity	P_{32} Low	P_{32} High	Color
None	0	0.00001	Blue
Low	0.00001	0.5	Green
Medium	0.5	1	Red
High	1	1+	Magenta

A benefit of calculating P_{32} fracture intensity for individual voxels is that it allows for a means of calculating the representative element volume of the DFN model. Liu *et al.* (2018) used the P_{32} values for sampled cubes with a DFN to determine the representative elementary volume (REV). The voxelization process here identifies the P_{32} intensity for all voxels on the Cartesian grid. These values can be used as proxies for the sampled values used by Lui *et al.* (2018). Figure 8 shows the relation between fracture intensity variability and block side length. The REV can be statistically identified using a Chi-square goodness-of-fit test.

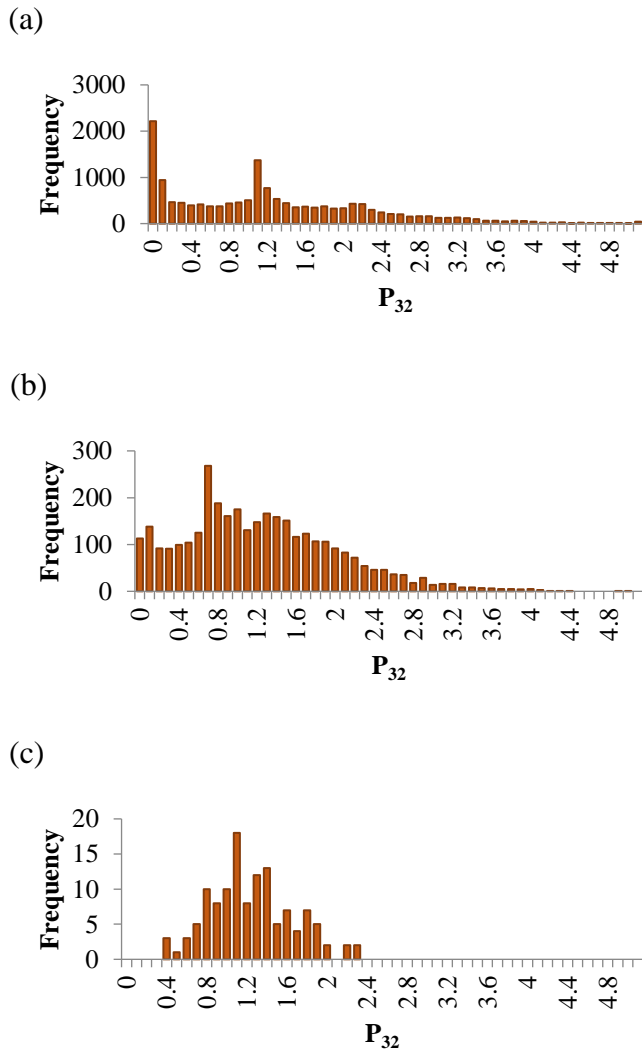


Figure 7. Three histograms showing changes in variability of P_{32} fracture intensity with the degree of voxelization for a single DFN realization. DFN discretization of $25 \times 25 \times 25$ (a), $15 \times 15 \times 15$ (b), and $5 \times 5 \times 5$ (c).

6. IN SITU BLOCK SIZE DISTRIBUTION (IBSD) ESTIMATION

The IBSD of a rock mass is an important variable used for rock mass characterization. New methods of calculating or estimating this parameter are of importance, and

complements rock mass classification systems such as RMR (Bieniawski, 1989), the Q system (Barton, *et al.*, 1974), and GSI (Hoek *et al.*, 1995), and can improve characterization techniques (Elmo *et al.*, 2014). The traditional methods of calculating average block size and distributions are reviewed by Maerz and Germain (1996), Lu (1997), and Palmström (2000). The traditional methods rely on many assumptions and generalizations in order to characterize a rock mass sufficiently to predict block sizes. Block size distributions are often determined numerically as a function of joint spacing and the number of fracture sets. It is a computationally expensive process to determine block sizes directly from a large three dimensional DFN model. A method of predicting the IBSD of a DFN model that is derived from the P_{32} voxelization is presented here.

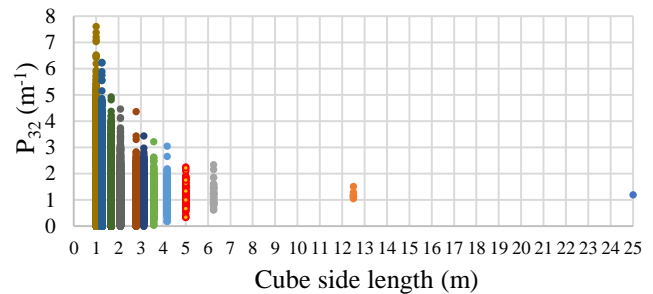


Figure 8 Volumetric fracture intensity variability for different cube sizes.

By calculating the P_{32} fracture intensity for all voxels in the DFN, the number of null blocks, that is, voxels with a fracture intensity of zero, can be quantified. With a set of null blocks within a DFN, an estimation of the IBSD can be made. Where a null block is identified, the IBSD algorithm searches the *6-adjacent* blocks that share a face with the known null block (Cohen-Or and Kaufman, 1995). This allows for the formation of compound blocks where neighboring blocks also contain no fractures.

The initial compound blocks tend to form highly concave geometries. The second part of the IBSD algorithm checks the density of a compound block by assigning a null block a value of 1; the fractured volume surrounding the compound block required to achieve convexity is assigned a value of 0. Figure 9 shows three examples of compound null blocks (in blue) and the associated densities. The empty space required to achieve convexity is fractured rock. The calculated density is the null block volume divided by the total volume. A density threshold is a required input for the IBSD algorithm. This threshold determines when compound blocks should be split due to concavities.

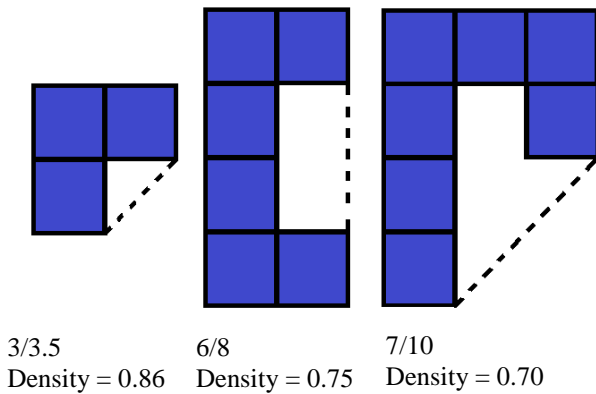


Figure 9. Density test for concave compound null blocks

Figure 10 shows the complete set of null blocks for a single DFN realization at different density thresholds. Thresholds of 0.4, 0.5, 0.6, 0.7, 0.8, and 0.9 were considered for the DFN model. The degree of block splitting can be seen by the number of colors when considering the entire model. A specific compound block is highlighted (in yellow) to demonstrate the effect of the block splitting thresholds. A density threshold of 0.4 results in one split of the compound block, whereas a density threshold of 0.9 results in 7 splits and 8 component blocks.

This feature is designed to allow for variation in the analysis of a DFN model that corresponds to the natural state of the rock mass. When a rock mass is massive and relatively unfractured, a lower threshold would be used. When a rock mass is very blocky and disturbed, a higher threshold would be appropriate.

The resulting block size distributions for each threshold are plotted in Figure 11. The IBSD of an intact rock mass can be expected to follow a power law relation (Lu, 1997; Srivastava, 2006). This information will be used to determine the optimum threshold for this particular DFN model by investigating the R^2 value for the power law equation that best fits the data. Although R^2 values may not be representative of a true power law distribution, they do give some indication of agreement with a power law distribution, especially when extreme values on the tail of the distribution are removed (Clauset, *et al.*, 2009). Where the R^2 value is highest, the data is best represented by a power law relation. This is a useful tool to determine what threshold to apply when there is no existing data on the state of the rock mass. Table 6 gives the R^2 values when considering all compound null blocks within the DFN model. The highest R^2 value achieved is 0.85 when considering a density threshold of 0.7.

When no fractures are seeded on the exterior surfaces of a volume, it is expected that there will be a lower fracture intensity on the boundaries. This boundary effect is seen in the visualization of blocks presented by Rogers *et al.*

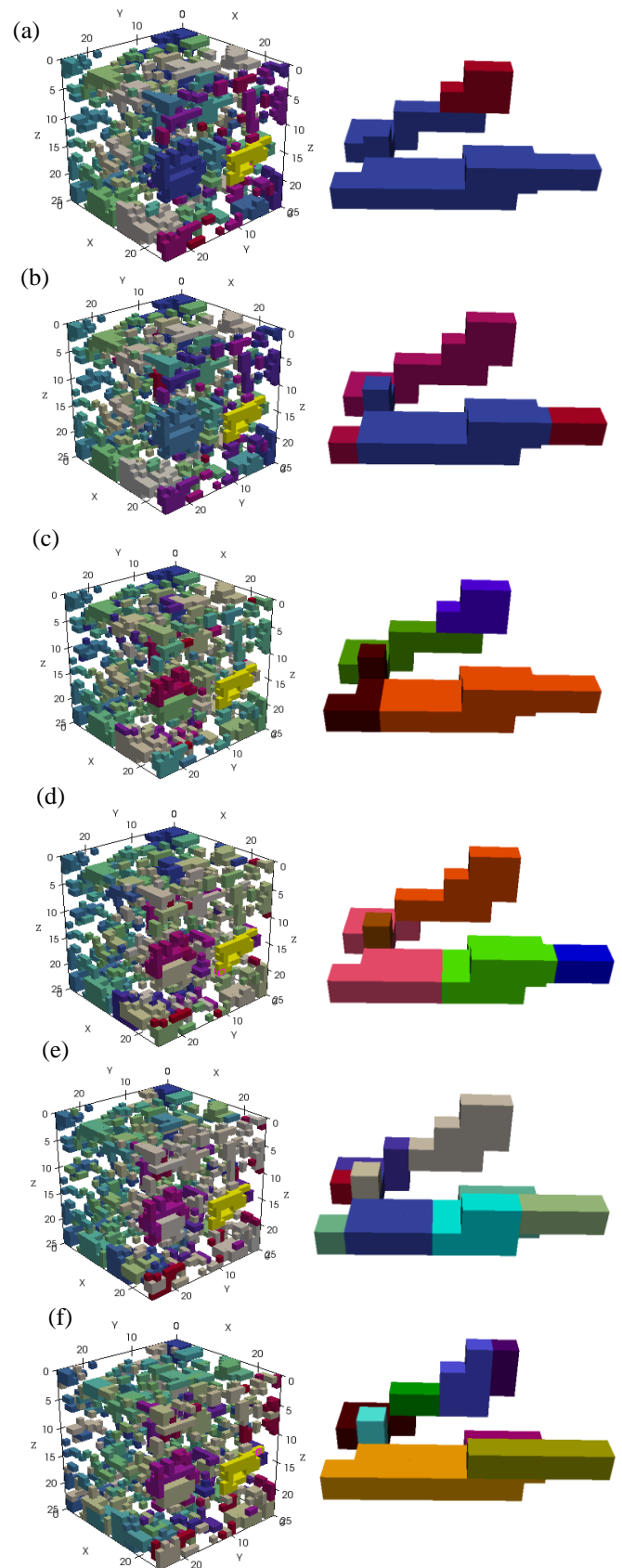


Figure 10. Determination of *in situ* block sizes using density thresholds of (a) 0.4, (b) 0.5, (c) 0.6, (d) 0.7, (e) 0.8, and (f) 0.9, with an example showing block subdivisions.

(2009), and can be seen in Figure 10, where the larger blocks are all near the boundaries of the model

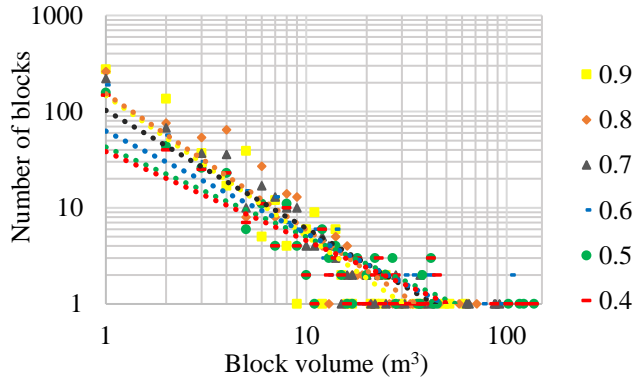


Figure 11. Block size distributions including all data for 6 block density thresholds.

Table 6. R^2 values for the best fit power law equation to the data including all blocks.

Block density	0.4	0.5	0.6	0.7	0.8	0.9
Power law R^2	0.71	0.73	0.74	0.85	0.83	0.80

In order to reduce the boundary effect on the estimated block size distribution, the blocks with a volume greater than 25 m^3 are removed from the dataset to give the plot presented in Figure 12. It can be seen that this causes a more distinct power law relationship between block size and frequency, which is demonstrated by the data concerning R^2 values presented in Table 7 for the best fit power law equation. With the arger boundary blocks removed from the dataset, the R^2 value is again highest for a 0.7 density threshold, with a value of 0.94.

As the density threshold of 0.7 yields the best fit to a power law relation when larger blocks are removed from the data, the values from this analysis are further investigated by plotting a percentage passing curve, presented in Figure 13. The minimum block size for this data is 1 m^3 , thus no blocks smaller than 1 m^3 will be accounted for.

Figures 12 and 13 show only the smaller blocks within the distribution; the extreme values on the tail of the distribution have been removed. To determine the block size distribution that includes blocks as small as 0.001 m^3 , would require a voxelization of 250 subdivisions per axis for a $25 \times 25 \times 25 \text{ m}^3$ DFN model. This would result in over 15 million voxels, which is computationally demanding. A more streamlined algorithm will allow for fracture intensities to be determined for higher resolutions

resulting in smaller voxels and thus giving information about smaller blocks belonging to the IBSD.

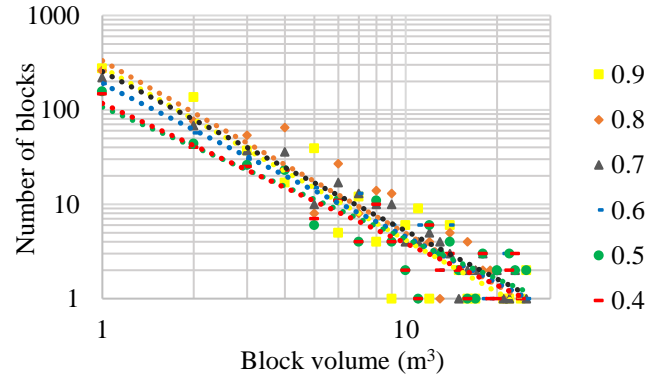


Figure 12. Block size distributions for all blocks less than or equal to 25 m^3 for 6 block density thresholds.

Table 7. R^2 values for the best fit power law equation to the data for blocks less than or equal to 25 m^3 .

Block density	0.4	0.5	0.6	0.7	0.8	0.9
Power law R^2	0.84	0.81	0.89	0.94	0.84	0.84

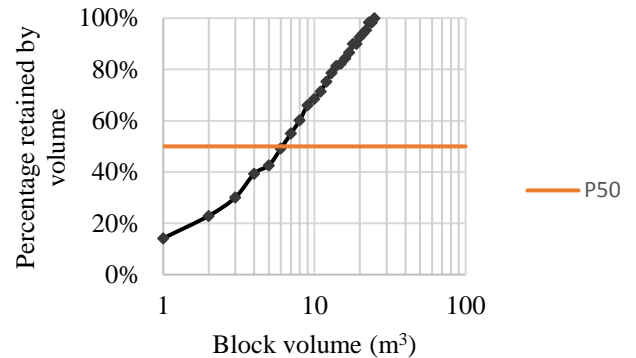


Figure 13. Block size distribution curve for a single realization of the DFN model with a block density threshold of 0.7, with all blocks greater than 25 m^3 removed from the dataset.

7. DISCUSSION

This research has allowed for detailed analysis of MoFrac-generated DFN models with respect to fracture intensity and fracture intensity variability. The method is based on voxelization, which allows for a DFN model to be discretized into component voxels, equivalent to a block model. This means of visualization is important to consider when generating mine-scale DFN models. The fracture intensity block model would add valuable information to existing block models that could relate to seismicity, blast design, and ground support (Elmo *et al.*, 2014).

Information on the heterogeneity of fracture intensity within a rock mass is important for a variety of applications. This includes engineering designs for buildings and excavations. Changes in fracture intensity play a major role in rock fragmentation by blasting, controlling how explosive energy passes through a rock mass (Dick, *et al.*, 1992). Consideration of terminations between fracture sets plays a significant role in the heterogeneity of fracture intensity in a DFN model. Future work will focus on relations between fracture sets and the resulting effect on fracture intensity variability.

The development of a CV% curve allows for a complete representation of fracture intensity variability within a DFN model. The CV% curve will be affected by the fracture intensity, orientation and the number of fracture sets. This curve can serve as a form of DFN model validation and can be used for calibration. Future work will include the comparison of CV% curves for a variety of DFN recipes. This will allow for further understanding of how primary DFN modeling properties affect the CV% curve.

An additional benefit of determining the P_{32} fracture intensity for component voxels of a DFN model is that the number and location of null blocks is also determined. This is useful information in terms of determining the IBSD of a rock mass. A single voxelization process is required to determine the IBSD, with the voxel size representing the smallest block size of interest. Future work will focus on streamlining the IBSD algorithm in order to handle voxel volumes less than 1 m^3 for large DFNs.

The key components of the IBSD algorithm are determining neighboring null blocks and the block splitting process. Having flexibility in determining the density threshold used for block splitting allows for this process to be tailored to specific rock mass conditions. This also leads to the possibility of modeling an excavation damaged zone (using a much higher density threshold in a specific DFN region surrounding excavations) together with an expected IBSD in the rock mass itself.

As there is a boundary effect associated with the DFN models generated for this paper, it was decided to eliminate the largest blocks from the data set which occurred along the boundaries. This was done in order to find the threshold that yielded data that best fit a power law relation. If fractures are allowed to be seeded close to the DFN region but out of bounds, or if fracture traces are used as seeds on the exterior boundaries of the DFN region, the boundary effect can be minimized.

The block splitting algorithm developed in this research is rudimentary at this point. The density threshold controls the splitting. A block is split once the density threshold is reached. Future work will develop the IBSD

algorithm to split blocks in ways that better match what would be expected in the field. For example, a large compound block would ideally be initially split at the weakest point of its geometry.

MoFrac and the built-in metrics are still in development; the software is intended to provide inputs such as IBSD and CV% of fracture intensity for secondary modeling, including flow analysis, slope stability studies, and blast fragmentation optimization. Visual and numerical outputs will be developed based on the discretization of DFN models using a voxelization approach.

8. ACKNOWLEDGMENTS

Special appreciation is given to Scott McGarvey, the lead developer of MoFrac at MIRARCO Mining Innovation. The impetus to this work was inspiring conversations with R. Mohan Srivastava of FSS Consultants Canada, Raymond Munier of SKB, and Frans Basson of Newmont Mining. The development of MoFrac is sponsored by the Nuclear Waste Management Organization (NWMO), and this work would not be possible without the support and feedback they provide.

9. REFERENCES

- Abdi, H. (2010) Coefficient of variation. In *Encyclopedia of Research Design*, ed. N. Salkind, Sage Publications Inc., 170-172.
- Alghalandis, Y and D Elmo (1988) Application of graph theory for robust and efficient rock analysis. *Proc. The 2nd International Discrete Fracture Network Engineering Conference (DFNE)*, American Rock Mechanics Association, Seattle, Washington, USA. 18-733.
- Barton, N., R. Lien, and J. Lunde (1974) Engineering classification of rock masses for the design of rock support. *Rock Mechanics*, 6:189-236.
- Bieniawski, Z.T. (1989) *Engineering rock mass classification*, 251 pp. New York, NY, Wiley.
- Cohen-Or, D and A. Kaufman. (1995) Fundamentals of surface voxelization. *Graphical Models and Image Processing*. 57(6):453-461.
- Clauset A, C.R. Shalizi, and M.E.J. Newman. (2009) Power-Law Distributions in Empirical Data. *SIAM Review*. 51(4):661
- Dershowitz, W.S. and H.H. Herda. (1992) Interpretation of fracture spacing and intensity. *Proc. The 33rd U.S. Symposium on Rock Mechanics (USRMS)*, American Rock Mechanics Association. Santa Fe, NM, USA. pp. 757-766.
- Dershowitz, W.S., A. Finnila, S. Rogers, P. Hamdi, and K.M. Moffit, (2017) Step path rock bridge percentage for analysis of slope stability. *ARMA 2017, San Francisco, CA*. 17-1045, 9 p.
- Dick, R.D., W.L. Fournery, X.J. Wang, C. Young, and Y. Wei. (1992) Mechanisms of fracture and fragmentation by explosive loading. Prepared for Air Force Office of Scientific Research, Bolling Air Force Base, Washington, DC.

Elmo, D., S. Rogers, D. Stead, and E. Eberhardt (2014) Discrete fracture network approach to characterise rock mass fragmentation and implications for geomechanical upscaling. *Mining Technology*, 123(3):149-161.

Hoek, E., P.K. Kaiser, and W.F. Bawden (1995) *Support of underground excavations in hard rock*, Rotterdam, A.A. Balkema.

Min, K-B., L. Jing, and O. Stephansson. (2004) Determining the equivalent permeability tensor for fractured rock masses using a stochastic REV approach: Method and application to the field data from Sellafield, UK. *Hydrogeology Journal*, 12: 497-510.

MIRARCO. (2019) MoFrac DFN Modelling Software, MIRARCO Mining Innovation, Sudbury, Canada. www.MoFrac.com.

Junkin, W.R., D. Janeczek, S. Bastola, X. Wang, M. Cai, L. Fava, E. Sykes, R. Munier and R.M. Srivastava. (2017) Discrete fracture network generation for the Äspö TAS08 tunnel using MoFrac. *ARMA 2017, San Francisco, CA*. 17-339, 10 p.

Junkin, W.R., L. Fava, E. Ben-Awuah and R.M. Srivastava. (2018) Analysis of MoFrac-generated deterministic and stochastic discrete fracture network models. *DFNE 2018, Seattle, WA*. 18-114, 10 p.

Latham, J-P., J. Van Meulen, S. Dupray (2006) Prediction of in-situ block size distributions with reference to armourstone for breakwaters. *Engineering Geology* 86:18-36.

Lu, P. (1997) The characterization and analysis of in-situ and blasted block size distributions and the blastability of rock masses. PhD thesis, Queen Mary, University of London.

Lui, Y., Q. Wang, J. Chen, S. Song, J. Zhan, and X. Han (2018) Determination of geometrical REV's based on volumetric fracture intensity and statistical tests. *Applied Sciences* 8:800-818.

Maerz N.H. and P. Germain (1996) Block size determination around underground openings using simulations. Proceedings of the *FRAGBLAST 5 Workshop on Measurement of Blast Fragmentation*, Montreal, QC, 23-24 August. pp. 215-223.

Medinac, F., T. Bamford, K. Esmaili and A.P. Schoelig (2018) Pre- and post-blast rock block size analysis using UAV-based data and discrete fracture network. *DFNE 2018, Seattle, WA*. 18-151, 9 p.

Palmström, A. (2000) Block size and block size distribution. Presented at workshop on *Reliability of classification systems* in connection with the GeoEng2000 conference, Melbourne, 18 – 24 November.

Rogers, S., Elmo, D., Beddoes, R. and Dershowitz, W. (2009) Mine scale DFN modelling and rapid upscaling in geomechanical simulations of large open pits, *International Symposium on Rock Slope Stability in Open Pit Mining and Civil Engineering, Santiago, Chile*. CD-ROM only, Day 2, 11 p.